Pharm Res (2011) 28:2505–2515
DOI 10.1007/s11095-011-0478-6

RESEARCH PAPER

Assessment of P-glycoprotein Activity in the Blood-Brain Barrier (BBB) Using Near Infrared Fluorescence (NIRF) Imaging Techniques

Ngoc H. On • Fang Chen • Martha Hinton • Donald W. Miller

Received: 1 December 2010 / Accepted: 10 May 2011 / Published online: 20 May 2011

ABSTRACT

Purpose To examine functional activity of P-glycoprotein (P-gp) in the blood-brain barrier (BBB) using near infrared fluorescence (NIRF) imaging techniques.

Methods Cellular accumulation and bi-directional permeability of the NIRF probe, rhodamine 800 (R800) was determined in MDCK*MDR1* and MDCKwt monolayers under normal conditions and following P-gp inhibition with GF120918. Functional P-gp activity was also assessed in mice following administration of R800 alone and with GF230918. Quantitative analysis of R800 fluorescence in brain tissue and blood was measured ex-vivo using Odyssey Near Infrared imaging.

Results R800 accumulation was reduced in MDCK*MDR1* compared to MDCKwt monolayers. Addition of GF120918, resulted in increased R800 accumulation in MDCK*MDR1* monolayers. Permeability of R800 in MDCK*MDR1* monolayers was significantly enhanced (4-fold) in the basolateral to apical direction under control conditions and was abolished following treatment with GF120918. With the exception of the choriod plexus, there was very little penetration of R800 into the brain under control conditions. Treatment of mice with GF120918 resulted in a nearly 4-fold increase in R800 fluorescence in the brain. In contrast, GF120918 had no effect on brain penetration of a vascular permeability marker.

Conclusions *In vitro* studies demonstrate the P-gp transporter properties of the NIRF probe R800. Preliminary *in vivo* studies confirm the P-gp transporter liabilities of R800 and suggest this probe may be useful as a molecular imaging agent for examining P-gp activity in the BBB.

N. H. On • F. Chen • M. Hinton • D. W. Miller (✉)
Department of Pharmacology & Therapeutics
University of Manitoba
753 McDermot Ave.
Winnipeg, Manitoba R3E 0T6, Canada
e-mail: miller5@cc.umanitoba.ca

KEY WORDS blood-brain barrier · near infrared fluorescence · P-glycoprotein · rhodamine 800

ABBREVIATIONS

ATP	adenosine triphosphate
BBB	blood-brain barrier
BCRP	breast cancer resistance protein
BCSFB	blood-cerebral spinal fluid barrier
CNS	central nervous system
MDCK	Madin-Darby Canine Kidney epithelial cell line
MDR	multidrug resistance
NIRF	near infrared fluorescence
PEG	poly(ethelene) glycol
PET	positron emission topography
P-gp	P-glycoprotein
R800	Rhodamine 800

INTRODUCTION

The delivery of many drugs for the treatment of central nervous system (CNS) disorders is limited by the presence of the blood-brain barrier (BBB). The BBB is comprised of a continuous layer of endothelial cells, associated astrocyte foot-processes and scattered pericytes. However, it is the brain microvessel endothelial cells with highly developed tight-junction complexes, low endocytic activity and the absence of fenestrations (1) that provide the physical barrier to the passage of most polar and hydrophilic solutes from the blood into the brain. In addition to restricted paracellular diffusion, the brain microvessel endothelial cells (BMEC) forming the BBB express numerous transporter systems that are essential for maintaining the proper brain microenvironment (2).

P-glycoprotein (P-gp) is a drug efflux transport protein that was originally identified in multidrug resistant cancer cells (3), but is also found in intestinal, kidney and liver epithelial cells and the BMEC of the BBB (4). A member of the ATP-binding cassette (ABC) family of proteins, P-gp actively transports a wide variety of drugs out of the cell (5). The expression of P-gp and related drug efflux transporters in the BBB has multiple implications on CNS response to drugs. The presence of P-glycoprotein activity in the BBB influences the brain distribution of a large number of therapeutic agents including anticancer drugs, antivirals, antihistamines, antiepileptics and analgesics (6–9). The wide range of drugs with P-gp transporter activity also poses potential problems with regard to drug interactions and unwanted brain penetration of therapeutic agents (10). A final consideration is the potential for altered P-gp expression and/or activity in the BBB in response to hypoxia (11), seizure activity (12) or drug exposure itself (13). For all the above, the ability to assess P-gp activity has important implications for understanding both drug- and pathology-induced changes in BBB permeability.

Positron emission tomography (PET) is a powerful imaging tool for assessing CNS function. Application of PET imaging to assess P-gp activity in the BBB has been performed with radiolabeled P-gp substrates including [^{11}C] verapamil, [^{11}C] cloperamide and [^{11}C] N-desmethyl loperamide in human and in animal studies (14,15). However, the highly specialized facilities and instrumentation required and the costs associated with PET imaging limit its general use. Therefore, alternative imaging techniques applicable to small animal pre-clinical studies are needed. Fluorescence and bioluminescence have been used for imaging studies, although tissue penetration is a major limitation (16,17). The development of near infrared fluorescence (NIRF) imaging techniques has emerged as an alternative to PET. The longer emission wavelength allows deeper tissue penetration (up to 2 or more centimeters compared to 1–2 mm with standard fluorescent imaging probes) (18). Additionally, background fluorescence in tissue and cells is low in the NIRF range (700–800 nm) (19). While there are a growing number of near infrared probes for various applications (20), there are no published reports of NIRF imaging agents for P-gp. Development of such probes would greatly facilitate application of NIRF imaging techniques for assessing P-gp function.

The purpose of the present study was to identify a suitable method for examining P-gp activity using NIRF imaging techniques. Rhodamine 800 (R800) is a lipophilic, cationic dye with a chemical structure similar to that of rhodamine 123 (R123), a P-gp substrate (21). Unlike the other rhodamine dyes, R800 has fluorescence emission properties in the NIRF range (685 to 730 nm wavelength). Based on these properties, rhodamine 800 (R800) was examined as a potential NIRF imaging probe for assessing P-gp activity in the BBB. Results of the present study demonstrate that R800 is indeed a P-gp transport substrate. The initial *in vivo* studies suggest R800 may be a suitable NIRF imaging agent for assessing P-gp activity in the BBB.

MATERIALS AND METHODS

Materials/Reagents

Rhodamine 800 was purchased from Exciton Inc. (Dayton, Ohio). The vascular and lymphatic NIRF imaging agent, IRdye 800cw PEG, was obtained from Licor (Omaha, NE). Elacridar (GF120918) was obtained from Toronto Research Chemical Inc. (Toronto, ON). Dulbecco's Modified Eagle's Medium, standard fetal bovine serum, non-essential amino acid solution, and 1X trypsin were purchased from HyClone (Logan, Utah). Penicillin-streptomycin was supplied by MP Biomedicals (Solon, Ohio). Ketamine hydrochloride and xylazine were purchased from Wyett (Guelph, ON) and Bayer Inc. (Toronto, ON), respectively. Transwell® polycarbonate membrane inserts (0.4 μm pore size; 24 mm diameter) were purchased from Corning Incorporated (Corning, NY). All other reagents and chemicals were purchased from Sigma Chemical Company (St. Louis, MO).

Cell Lines

Madin-Darby canine kidney epithelial cells (MDCK) were purchased from American Type Tissue Culture Collection (Manassas, VA), and MDCK cells transfected with the human *MDR1*gene were provided by M. Gottesman, National Cancer Institute (Bethesda, MD). The cells were grown in Dulbecco's Modified Eagle's Medium (DMEM) supplemented with 10% standard fetal bovine serum, 1% penicillin-streptomycin and 1% non-essential amino acids. The MDCK*MDR1* were grown in the same media as described above with the addition of (0.2 μM) colchicine to maintain elevated expression of P-glycoprotein. Cells were expanded in 75 cm^2 culture flasks and seeded onto 12-well culture plates or Transwell® inserts at a density of 50, 000 cells per cm^2 for uptake and permeability studies, respectively. Cells were grown in a humidified environment of 37°C with 5% CO_2 with media replacement every other day.

Accumulation Studies

Confluent monolayers of MDCKwt and MDCK*MDR1* cells were grown in a 24-well plate and pre-treated for 30

min at 37°C with 0.5 ml assay buffer (AB, containing in mM; 122 NaCl, 3 KCl, 1.4 $CaCl_2$, 1.2 $MgSO_4$, 25 $NaHCO_3$, 10 HEPES, 10 glucose, and 0.4 K_2HPO_4 at a pH of 7.4) with or without 1 μM GF120918. Following pre-treatment, solutions were removed and replaced with AB containing 3.2 μM of R800 with or without 1 μM GF120918. Cells were incubated for various time points (15–60 min) at 37°C, after which the solutions were aspirated, and the cells were washed 3 times with 0.5 ml/well of ice-cold phosphate-buffered saline solution (145 mM NaCl, 3 mM NaH_2PO_4, and 7 mM Na_2HPO_4) and then solubilized with 0.5 ml/well of 1% Triton-X 100. The amount of R800 in MDCKwt and MDCK*MDR1* cells under control and GF-120918-treated conditions were normalized to the amount of protein present in cell lysates and determined using an Odyssey Near Infrared Imaging System (LI-COR Biosciences, Lincoln, Nebraska) set on the 700 nm channel.

Bi-Directional Permeability Studies

Permeability was assessed over a 60-min period in both MDCKwt and MDCK*MDR1* monolayers in the apical to basolateral (A to B) and basolateral to apical (B to A) directions. The volume of the apical compartment was 1.5 ml, and the volume in the basolateral compartment was 2.5 ml. The initial concentration of R800 in the donor compartment was 10 μM. Samples were removed from the donor compartment (10 μl) at the start of the study. Samples were also taken from the receiver compartment (150 μl) at various times over a 60-min period. In separate studies, bi-directional permeability of R800 was also determined following a 30-min pre-treatment with the P-gp inhibitor, GF120918 (1.0 μM). All samples removed were replaced with an equal volume of assay buffer, and all permeability studies were performed at 37°C. Samples were analyzed as described above using the Odyssey near infrared fluorescence imager (LI-COR Bioscience, Lincoln, Nebraska), and the apparent permeability coefficients (P_{app}) were determined based on the following formula:

$$P_{app} = dC_r/d_t(V_d/A*C_d)$$

where C_r is concentration in the receiver compartment, t is time, V_d is the volume in the donor compartment, A is the area, and C_d is the concentration in the donor compartment at time 0.

The efflux ratio (ER) was determined by dividing the P_{app} for R800 in basolateral to apical (B–A) direction by the P_{app} for R800 in the apical to basolateral (A–B) direction as described previously (32,33).

P-gp ATPase Assay

R800-induced ATP hydrolysis was assessed using High Five insect cell membranes expressing human MDR1, BCRP and MRP1 (BD Bioscience). A 0.06 mL reaction mixture containing 20 μg membranes, 20 μM verapamil (positive control) or various concentrations of R800 (1–10 μM) and 5 mM MgATP, in buffer containing 50 mM Tris-MES, 2 mM EGTA, 50 mM KCl, 2 mM dithiothreitol, and 5 mM sodium azide, was incubated at 37°C for 20 min in the presence or absence of sodium orthovanadate (22). Orthovanadate inhibited P-gp-dependent ATP hydrolysis by trapping MgADP in the nucleotide binding site. Thus, ATPase activity measured in the presence of orthovanadate was subtracted from the activity generated without orthovanadate to yield vanadate-sensitive ATPase activity. The reaction was stopped by the addition of 30 μL 10% sodium dodecyl sulfate (SDS) with antifoam A. An additional 20 min incubation at 37°C was performed following the addition of 200 μL of 35 mM ammonium molybdate in 15 mM zinc acetate in 10% ascorbic acid (1:4). The liberation of inorganic phosphate resulting from the addition of P-gp transport substrate was detected through absorbance at 630 nm using a Synergy HT plate reader and quantitated by comparing the absorbance to a phosphate standard curve. The EC_{50}, K_m and V_{max} values from the ATPase studies were determined using a sigmoidal dose-response nonlinear regression curve fit of the experimental data performed by GraphPad Prism version 3.02 (GraphPad Software, San Diego, California).

R800 Tissue Distribution in Mice

Adult female Balb/c mice were obtained from the University of Manitoba breeding colony and maintained in the Central Animal Care Facility under temperature-controlled environment with 12 h dark/light cycle and unlimited access to food and water. All animal experiments were approved by the University of Manitoba Animal Care Committee (protocol number 08–0866).

Female Balb/c mice were anesthetized with a cocktail of ketamine and xylazine. Mice were administered R800 (0.032 μmol/kg) either alone or in combination with the vascular permeability marker, IRDye 800cw (0.01 μmol/kg), via tail vein injection. To determine the effects of P-gp on R800 and IRDye 800cw PEG tissue accumulation, a separate group of mice received 9 mg/kg of GF120918 via tail vein injection 15 min prior to administration of the imaging agents. Previous studies have shown this dose and dosing schedule for GF120918 to produce plasma concentrations of GF120198 above the IC_{50} of the compound throughout the entire period of study. Stock solutions of GF120918 and R800 were prepared in dimethyl sulfoxide

(DMSO) and diluted using 70% ethanol (GF120918) or phosphate-buffered saline (R800) so that the final concentration of DMSO was less than 1%. The IRDye 800cw PEG solutions were prepared directly in phosphate-buffered saline. Mice were sacrificed 20 min after administration of fluorescent imaging agents via cardiac perfusion with a 10% formaldehyde solution. Blood and tissue samples were collected and prepared for *ex vivo* imaging for R800 and IRDye 800cw PEG fluorescence using an Odyssey Near Infrared Fluorescence Imaging system. Fresh tissue was sectioned into 2 mm thick slices for *ex vivo* analysis. *In vivo* NIRF imaging was performed on both control and GF120918-treated mice prior to sacrifice to obtain whole animal scans at various times using the Odyssey Near Infrared Fluorescent Imaging system.

Statistical Analysis

The *in vitro* studies examining R800 accumulation and permeability were analyzed using ANOVA with Student Newman-Keul post-hoc comparison of the means. Changes in R800 fluorescence in the *ex vivo* tissue slice studies were analyzed using Student T-tests. Statistical significance was set at $p<0.05$ unless otherwise noted.

RESULTS

ATPase Studies

To examine whether R800 was a P-gp substrate, studies were performed using P-gp, BCRP, and MRP1 membranes (Fig. 1a). In these studies, hydrolysis of ATP was used as a quantitative index of drug efflux transporter activity. The results from the P-gp ATPase assay showed that R800 produced a clear dose-dependent increase in ATP hydrolysis (Fig. 1b). The resulting EC_{50} with R800 in the P-gp membrane assay was approximately 7 μM. In contrast, R800 added to the BCRP and MRP1 membrane preparation displayed no clear concentration dependency (Fig. 1a).

Accumulation and Permeability Studies in MDCKMDR1 Cells

Accumulation of R800 was examined in both MDCKwt and MDCK*MDR1* cell lines (Fig. 2a). The accumulation of R800 was significantly lower in the MDCK*MDR1* cells compared to the wild-type cells ($p<0.05$) at all time points examined, with the greatest differences observed at the 45 and 60 min time points (Fig. 2a). Treatment of the MDCK*MDR1* cells with GF120918 resulted in a significant

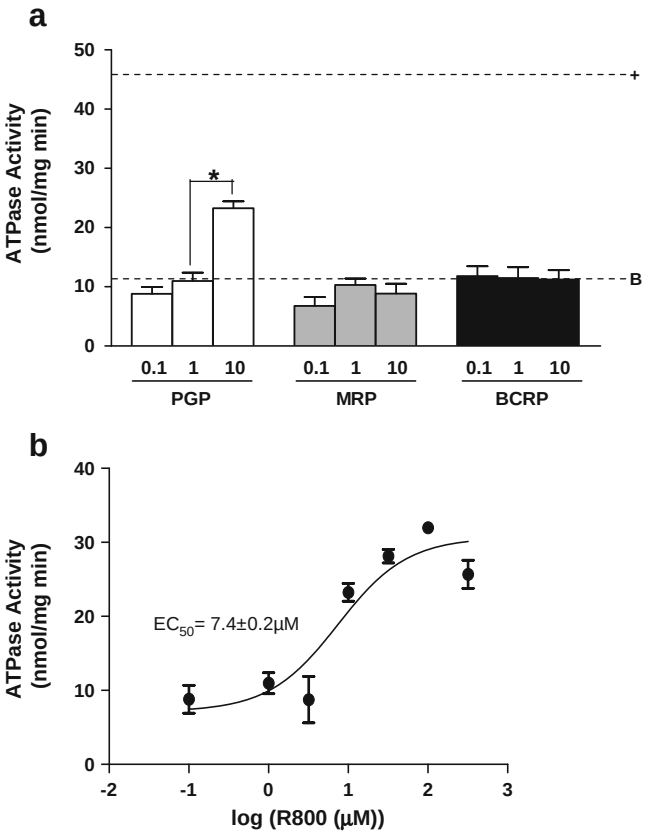

Fig. 1 Membrane ATPase studies with R800. ATPase activity in P-gp, MRP1 and BCRP membranes following exposure to 0.1, 1 and 10 μM R800 (**a**). *Dashed lines* represent basal (non-stimulated) activity (B) and response in P-gp membranes to 20 μM verapamil (+). Extended concentration response curve for R800 in P-gp membrane preparation (**b**). Values represent the mean ± SEM of 4 membrane preparations. * $p<0.05$ compared to basal activity. Curve fitted using Graphpad Prism software 3.02.

enhancement in R800 accumulation in the cells (Fig. 2a). Following treatment of the MDCK*MDR1* with GF120918, cellular levels of R800 were comparable to those observed in the MDCKwt cells under normal conditions. Qualitatively similar data were obtained using NIRF microscopy studies with the MDCK*MDR1* cells showing little R800 fluorescence under control conditions (Fig. 2b) and substantially higher levels of fluorescence following treatment with GF120918 (Fig. 2c).

Fig. 2 Cellular accumulation of R800 in MDCK*wt* and MDCK*MDR1* ▶ monolayers. Time-dependent accumulation of R800 in MDCKwt and MDCK*MDR1* cells in the absence and presence of 1 μM GF120918 (**a**). Fluorescence micrographs of R800 in MDCK*MDR1* cells following a 30 min exposure to 3.2 μM R800 alone (**b**) or 3.2 μM R800 together with 1.0 μM GF120918 (**c**). Values represent the mean ± SEM of 3 monolayers per time point and treatment group. * $p<0.05$ compared WT at the same time point.

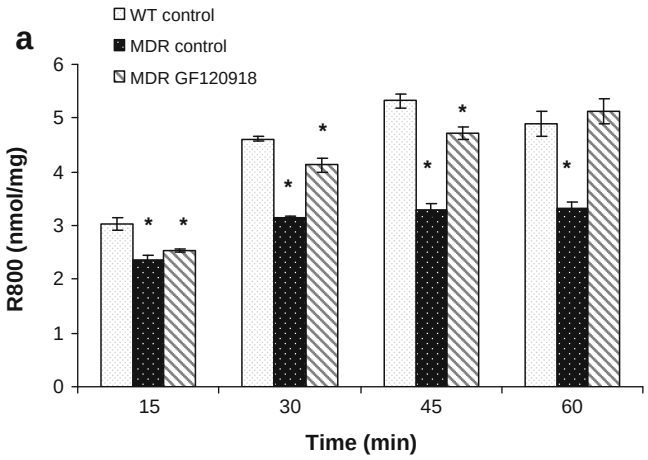

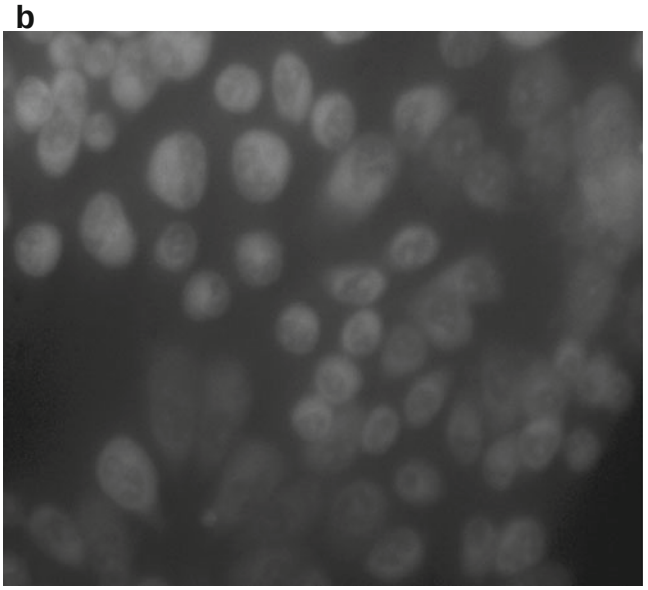

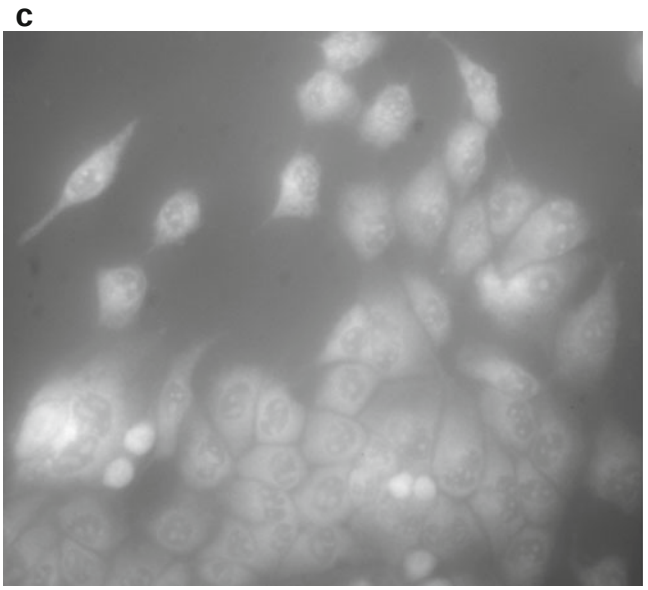

The bi-directional transport of R800 was also examined in MDCK*MDR1* monolayers. Under normal conditions (control), permeability was significantly greater in the basolateral to apical (B–A) direction compared to that observed in the apical to basolateral (A–B) direction (Fig. 3a). As a result, the efflux permeability ratio for R800 was approximately 3 in MDCK*MDR1* monolayers (Fig. 3b). In contrast, MDCK*MDR1* monolayers treated with GF120918 displayed similar permeability in both the B–A and A–B directions (Fig. 3a) and had an efflux permeability ratio near 1 (Fig. 3b).

R800 Tissue Distribution in Mice

The accumulation of R800 in the brain following systemic administration of the imaging dye was examined in mice under normal conditions and following treatment with P-gp inhibitor (GF120918). Representative brain slices from

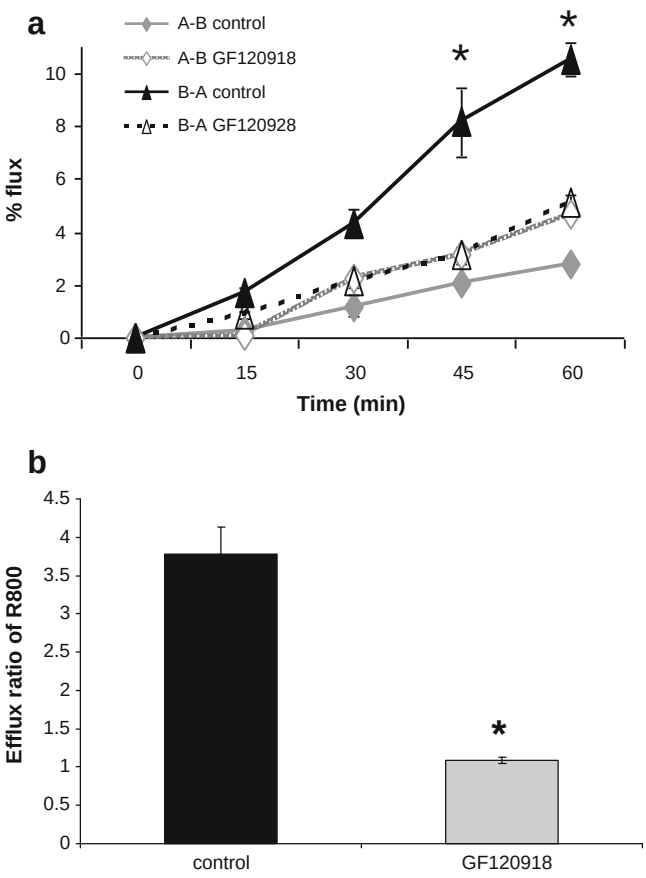

Fig. 3 R800 permeability studies in MDCK*MDR1* monolayers. Bi-directional permeability studies for R800 in MDCK*MDR1* cells in the presence and absence of GF120918 (**a**). Efflux ratio (ER) values for R800 under control conditions and following treatment with GF 120918 (**b**). The ER values were based on apparent permeability coefficients determined at 60 min. Values represent the mean ± SEM of 3 monolayers per treatment group. * $p < 0.05$ compared to A–B control monolayers; * $p < 0.05$ compared to ER in control group.

mice receiving either vehicle (PBS), R800, or R800 with GF120918 pretreatment are shown in Fig. 4. Under normal conditions, with functional P-gp, R800 accumulation in the brain is negligible, as indicated by the similar fluorescence in brain slices from R800-treated and vehicle injected mice receiving no R800 (Fig. 4a and b). Indeed, the only brain region showing appreciable accumulation of R800 was the ventricles, which showed intense fluorescence following i.v. injection of R800 (Fig. 4b). In contrast, following pretreatment with GF120918, the amount of R800 accumulating in brain tissue was substantially enhanced compared to both non-treated mice and mice receiving R800 alone (Fig. 4c). Quantitative assessment of R800 fluorescence in the brain and choroid plexus indicated an approximately 4-fold and 2-fold increase in fluorescence in the GF120918 pretreatment group, respectively, compared to control mice receiving R800 alone (Fig. 5a). In contrast, the vascular permeability marker IRdye 800cw PEG showed no appreciable brain accumulation in either control or GF120918 pre-treated mice (Fig. 6). Whole animal imaging indicated accumulation of R800 in both the liver and kidney within 7 min and even greater accumulation at 40 min following the injection (Fig. 7). The accumulation of R800 in the liver was enhanced in mice treated with GF 120918 (Fig. 7). Similar findings were observed in the *ex vivo* assessment of R800 fluorescence in liver and kidney slices, with a 2-fold enhancement of fluorescence in the liver of GF120918 treated mice (Fig. 5b). The fluorescence intensity in the kidney was not significantly influenced by GF120918 treatment (Fig. 5b).

DISCUSSION

It is well established that the drug efflux transporter, P-gp, plays an important role in the absorption, distribution, and excretion of a number of drugs (23). Of particular importance is the emerging role that P-gp has in limiting the central nervous system penetration of drugs (24). Given the potential for altered P-gp activity, either through a particular pathological condition, such as epilepsy (25), or through drug treatment regiments (26), a non-invasive method for imaging changes in P-gp activity, both quantitatively and spatially, in the BBB would provide an essential research tool. Traditionally, P-gp imaging in both the pre-clinical and clinical setting has been done using positron emission tomography (PET) and radiolabeled

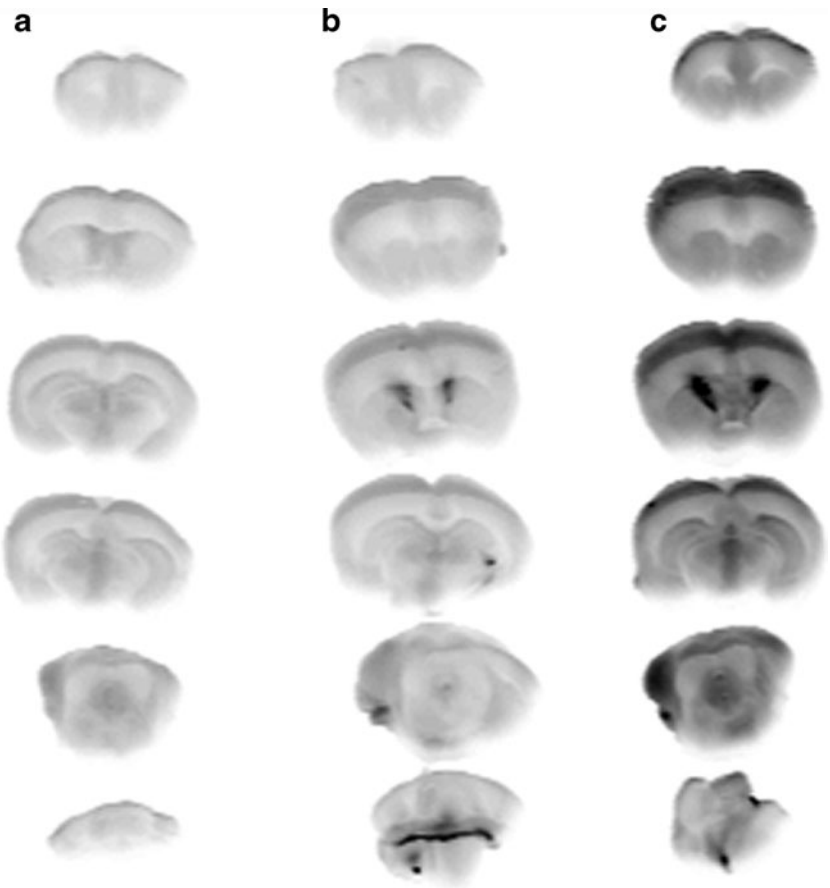

Fig. 4 Representative serial coronal slices of mouse brain from (**a**) control, (**b**) R800 treated, (**c**) GF120918 and R800 treated mouse at 20 min post injection. Slices were 2 mm thick and are oriented from the anterior (*top*) to posterior (*bottom*) regions. The darker the slice image, the greater the R800 fluorescence.

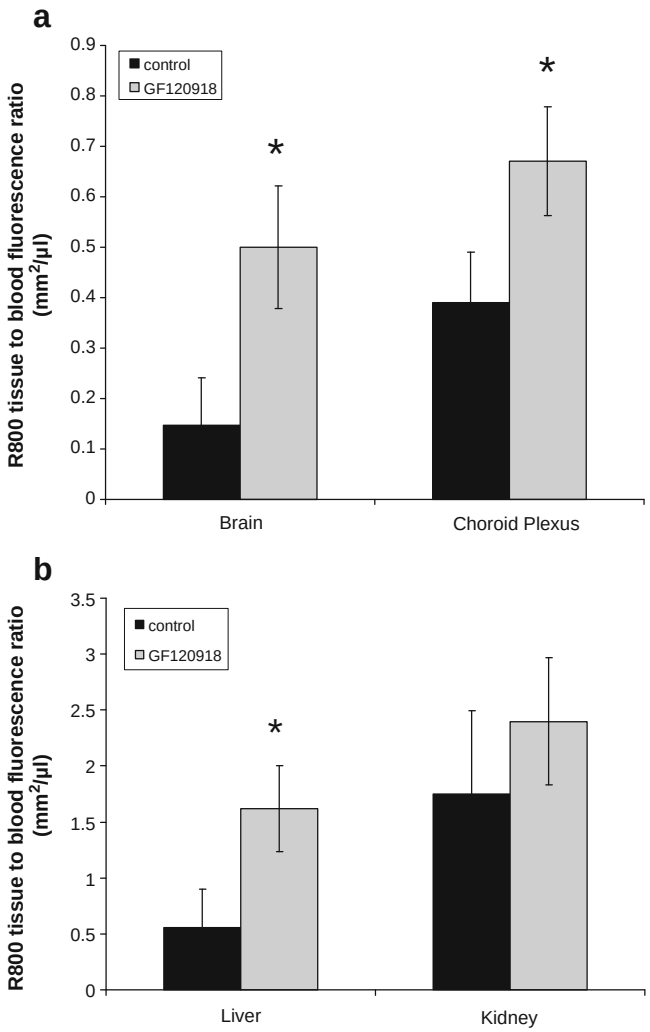

Fig. 5 Quantitative assessment of R800 fluorescence in the brain and choroid plexus (**a**), liver and kidney (**b**) under control conditions (R800 alone) and following pre-treatment with P-gp inhibitor, GF 120918. Fluorescence intensity is presented as tissue-to-blood ratio. Values represent the mean ± SEM ($n = 4$) of mice per treatment group. * $p < 0.05$ compared to control mice.

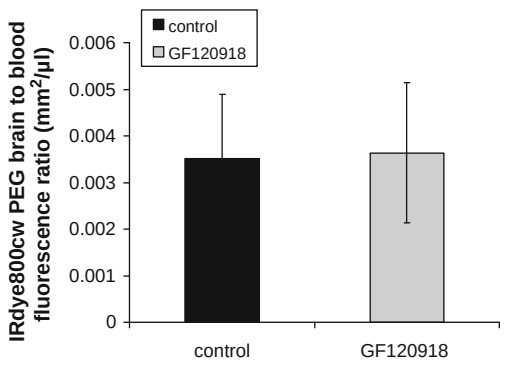

Fig. 6 Quantitative analysis of IRdye800cw PEG in the brain under control conditions and following pre-treatment with P-gp inhibitor, GF 120918. The total fluorescence from serial coronal brain slices were normalized to the fluorescence intensity of the blood. The values represent the mean ± SEM of ($n = 4$) mice per treatment group.

substrates of P-gp such as [^{11}C] verapamil (14). While PET imaging is a powerful technique, it requires highly specialized instrumentation and support facilities and can be cost prohibitive, especially in the pre-clinical setting. Thus, there is a need for the development of alternative imaging modalities.

Near infrared fluorescence represents an emerging imaging technology (27). The long absorption wavelengths (700–800 nm) in the NIRF region result in reduced background or autofluorescence within tissue. In addition, compared to fluorescence imaging within the visible spectrum that has a tissue penetration depth limited only to 1–2 mm, NIRF can penetrate up to several centimeters (18). Furthermore, the ability to utilize NIRF probes from the cellular to whole animal level provides an integrated imaging platform. In the present study, we report the initial identification and characterization of the NIRF probe, R800, as a potential imaging agent for assessing P-gp function at both the cellular and whole animal level.

The assessment of P-gp function using NIFR imaging technology required identification of a suitable compound with P-gp activity. Due to their planar ring structure, positive charge, and fluorescent properties, the rhodamine dyes, most notably rhodamine 123, have been utilized for functional assessment of P-gp (21,28–30). While the NIRF dye, R800, has some structural similarities to rhodamine 123, interactions of R800 with P-gp or other drug efflux transporters have not been reported. To assess whether R800 was indeed a P-gp substrate, a series of *in vitro* studies were performed. Cellular accumulation of R800 was performed using MDCKwt monolayers and MDCK*MDR1* monolayers. The MDCK*MDR1* transfected cell line over-expresses P-gp, and the utility of these cells in examining P-gp-dependent transporter processes has been well documented (31). There are two lines of evidence that suggest R800 is a substrate for P-gp in the cell accumulation studies. First, R800 had a significantly lower accumulation in the MDCK*MDR1* cells compared to the wild-type cells. Second, treatment with the P-gp inhibitor, GF120918, was able to bring R800 accumulation in the MDCK*MDR1* cells to the same level as the MDCKwt monolayers.

Additional evidence supporting R800 as a transport substrate for P-gp comes from the bi-directional permeability studies in the MDCK*MDR1* monolayers. Determination of permeability in both the A–B and B–A directions has been extensively utilized to identify compounds with drug efflux transporter liability (32). For compounds that are only dependent on passive diffusion processes, permeability across polarized epithelial cells would be expected to be similar in both directions. However, those compounds dependent on transport processes will display bi-directional permeability differences. In the case of P-gp-mediated transport, an increased B–A permeability is observed (33).

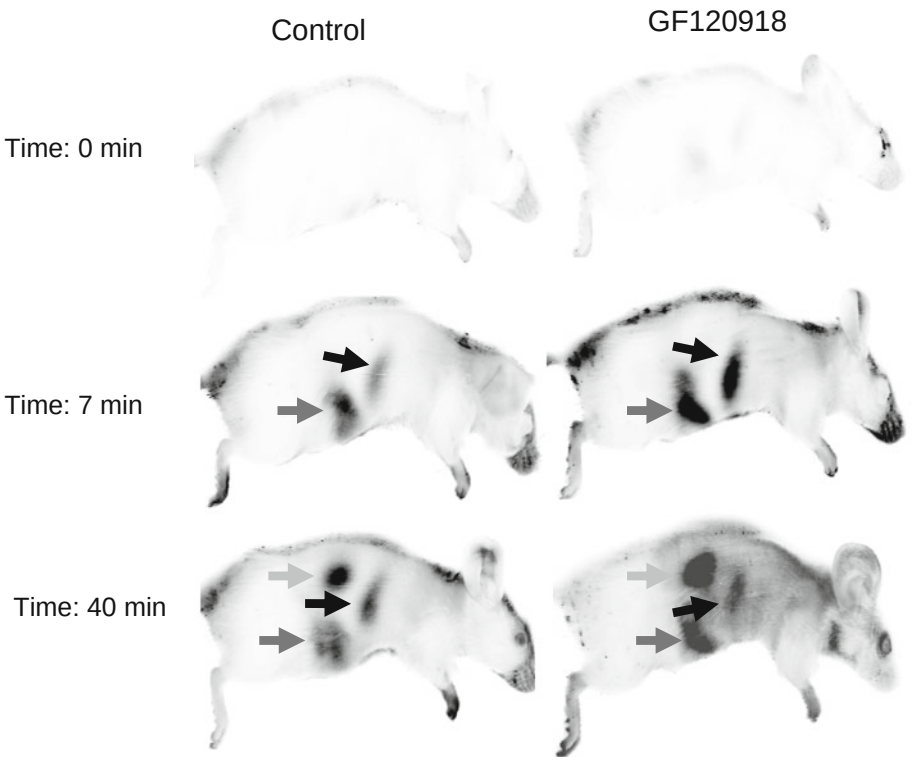

Fig. 7 Whole animal images of R800 tissue deposition in mouse using NIRF imaging. Images of control and GF120918 treated mice were taking at time 0, 7, and 40 min following R800 injection. Mice were positioned on side for R800 imaging. The arrows indicate accumulation of R800 in peripheral organs including liver (*black arrow*), intestines (*dark gray arrow*) and kidney (*light gray arrow*).

As observed in the present study, R800 permeability in MDCK*MDR1* monolayers was significantly greater in the B–A direction compared to that observed in the A–B direction. This resulted in an efflux ratio for R800 in MDCK*MDR1* monolayers of approximately 3. This is above the typical cut-off value of 2 used to identify drug efflux transporter liabilities in drug screening assays (34). Addition of the P-gp inhibitor, GF120918, resulted in a similar permeability of R800 in both the B–A and A–B directions.

Finally, confirmation that R800 is transported by P-gp comes from the membrane ATPase studies. P-glycoprotein-dependent transport requires the binding of the substrate to the transporter and subsequent hydrolysis of ATP via the ATPase portion of the transporter (32). Therefore, the screening of prospective substrates or inhibitors of P-gp can be determined by examining the amount of free phosphate generated through the activity of ATPase (32). The use of specific membranes that overexpress P-gp enables researchers to look at the interaction between a potential substrate and P-gp transporter without other confounding factors such as other efflux/influx transporters or permeability through an intact cell monolayer that can mask drug efflux transporter activity. In the present study, R800 produced a concentration-dependent increase in P-gp ATPase activity. The EC_{50} for R800 in the P-gp ATPase assay was 7 μM. This is similar to the 3 μM EC_{50} values reported previously for rhodamine 123 (35,36). In contrast to the P-gp ATPase membrane assay, no clear concentration-dependent response to R800 in was observed in the BCRP or MRP1 ATPase membrane preparation, suggesting that transport through these drug efflux systems is modest at best.

Based on *in vitro* studies demonstrating that R800 was a P-gp substrate, *in vivo* studies were initiated to determine to what extent R800 could be used to image P-gp function. Whole animal imaging of R800 distribution showed marked accumulation in both the liver, kidney and intestinal tissue, which was enhanced in the GF120918-treated mice. This is consistent with the important role that P-gp has in the elimination of compounds in these tissues. In this regard, these whole mouse images are similar to what has been reported previously with P-gp probes using PET (37). While whole animal imaging of P-gp function in the CNS was unsuccessful due in part to the autofluorescence from hair follicles in this particular preparation, significant and robust changes in P-gp activity in the brain were observed in the *ex vivo* setting. Examination of brain slices from mice following systemic administration of R800 indicated very little penetration of R800 into the brain. Indeed, under normal conditions, the brain region with the greatest R800 retention was the ventricles. However, following blockade of P-gp with GF 120918, there was a significant enhancement in R800 fluorescence in the brain slices (approximately 4-fold). The enhanced R800 accumulation in the brain slices from GF120918-treated mice in the current study is consistent with the approximately 3-fold increase in brain accumulation reported previously for rhodamine 123 following P-gp inhibition in rats using brain

microdialysis (28). While GF120918 can also inhibit BCRP transporter activity, the absence of effect in the BCRP membrane ATPase assay suggests the increases in fluorescence observed in the brain slices following GF120918 is attributable to P-gp inhibition.

Additional evidence that the enhanced R800 accumulation in the brain following GF120918 is due to inhibition of P-gp at the BBB is the lack of response observed with IRdye 800cw PEG contrast agent. This compound is a near infrared agent used previously to visualize the permeability of leaky or discontinuous vascular endothelium and lymph node mapping (38). The encapsulated portion of the molecule consists of Poly(ethylene glycol) PEG, a synthetic polymer that is commonly used to enhance the retention time or to alter the pharmacokinetics of an agent. The molecular weight of IRDye 800cw PEG is approximately 25 kDa. Based on the physicochemical properties of IRDye 800cw PEG, this imaging agent was selected to evaluate the specificity of the response to the P-gp inhibitor, GF120918. As expected from the physicochemical properties of the imaging agent, systemic administration of IRdye 800cw PEG resulted in little to no detectable accumulation in the brain and the choroid plexus region. In addition, treatment with GF120918 had no effect on the accumulation of IRdye 800cw PEG in brain tissue, indicating the effects observed with GF120918 in the R800-treated mice was due to inhibition of P-gp-mediated transport at the BBB.

In addition to the brain endothelial cells, P-gp is also expressed in the epithelial cells of the choroid plexus (39). Bidirectional permeability studies using neonatal rat choroid plexus epithelia along with radiolabeled probes ^{99m}Tc-sestamibi and ^{3}[H]Taxol showed that the permeability of P-gp substrates in the basolateral to apical direction was greater than permeability in the apical to basolateral direction (40). Furthermore, the enhanced basolateral to apical permeability was abolished when the choroid plexus epithelial cells were treated with GF120918 (40). The directionality of P-gp transport in the blood-cerebral spinal fluid barrier (BCSFB) is such that P-gp substrates would be concentrated in the cerebral spinal fluid (CSF) of the ventricles while just the opposite occurs in the BBB with the removal of P-gp substrates from the brain exrtacellular fluid (41). The apical localization of P-gp in the choroid plexus epithelial cells would account for the strong R800 fluorescence signal observed in the central ventricles following systemic administration of the dye. These finding are in good agreement with previous studies using PET imaging methods demonstrating a localization of P-gp PET probes in the ventricles (15). Thus, the brain accumulation of R800 observed under control conditions is consistent with the different orientations of P-gp in the BBB and BCSFB. When P-gp was inhibited, by the administration of GF120918, the amount of R800 in the brain was dramatically increased while the fluorescence in the ventricles only increased modestly. This is consistent with inhibition of P-gp in the BBB. The increase in R800 in the ventricles following GF120918 is attributable to diffusion of R800 from the brain extracellular fluid pool to the cerebral spinal fluid pool. Such a phenomenon has been shown for doxorubicin brain distribution following P-gp inhibition (42). In these studies, doxorubicin concentrations were monitored in both the brain cortex and ventricles using brain microdialysis. Thus, the results with the newly identified NIRF imaging agent in the present studies resemble the more established techniques for assessing P-gp function in the BBB and BCSFB.

Due to its localization within the body, P-gp can influence the bioavailability and tissue distribution of a wide range of compounds. Changes in P-gp activity either due to specific disease state or particular drug regimen have the potential to alter pharmacodynamics of P-gp-sensitive drug agents (43). Furthermore, transporter-mediated drug-drug interactions are also of growing concern (44). A non-invasive approach for examining the activity of P-gp would be of value for understanding the role of P-gp in both the above-mentioned conditions. While additional studies are required, this initial report suggests NIRF spectroscopy with imaging agents like R800 may provide an additional tool for monitoring changes in P-gp activity and drug distribution in tissues including brain.

CONCLUSIONS

The present studies represent the first demonstration of the use of NIRF to capture P-gp activity. The probe utilized shows strong P-gp activity in both *in vitro* and *in vivo* models. While non-invasive live animal imaging of P-gp activity in the BBB is currently ongoing, the images from the current study support the applications of NIRF spectroscopy for quantitative assessment of P-gp activity in the BBB and other tissue sites.

ACKNOWLEDGMENTS

This study was supported by Manitoba Health Research Council (MHRC) and National Science and Engineering Research Council of Canada.

REFERENCES

1. Girardin F. Membrane transporter proteins: a challenge for CNS drug development. Dialogues Clin Neurosci. 2006;8(3):311–21.
2. de Boer AG, Gaillard PJ. Blood-brain barrier dysfunction and recovery. J Neural Transm. 2006;113(4):455–62.

3. Matsuoka Y, Okazaki M, Kitamura Y, Taniguchi T. Developmental expression of P-glycoprotein (multidrug resistance gene product) in the rat brain. J Neurobiol. 1999;39(3):383–92.
4. Balayssac D, Authier N, Cayre A, Coudore F. Does inhibition of P-glycoprotein lead to drug-drug interactions? Toxicol Lett. 2005;156(3):319–29.
5. Ernst R, Kueppers P, Stindt J, Kuchler K, Schmitt L. Multidrug efflux pumps: substrate selection in ATP-binding cassette multidrug efflux pumps–first come, first served? FEBS J. 2010;277 (3):540–9.
6. Lin JH, Yamazaki M. Role of P-glycoprotein in pharmacokinetics: clinical implications. Clin Pharmacokinet. 2003;42 (1):59–98.
7. Lee CA, Cook JA, Reyner EL, Smith DA. P-glycoprotein related drug interactions: clinical importance and a consideration of disease states. Expert Opin Drug Metab Toxicol. 2010;6(5):603–19.
8. Bachmeier CJ, Spitzenberger TJ, Elmquist WF, Miller DW. Quantitative assessment of HIV-1 protease inhibitor interactions with drug efflux transporters in the blood-brain barrier. Pharm Res. 2005;22(8):1259–68.
9. Schinkel AH, Wagenaar E, Mol CA, van Deemter L. P-glycoprotein in the blood-brain barrier of mice influences the brain penetration and pharmacological activity of many drugs. J Clin Invest. 1996;97(11):2517–24.
10. Feng B, Mills JB, Davidson RE, Mireles RJ, Janiszewski JS, Troutman MD, *et al. In vitro* P-glycoprotein assays to predict the *in vivo* interactions of P-glycoprotein with drugs in the central nervous system. Drug Metab Dispos. 2008;36(2):268–75.
11. Callaghan R, Crowley E, Potter S, Kerr ID. P-glycoprotein: so many ways to turn it on. J Clin Pharmacol. 2008;48(3):365–78.
12. Pekcec A, Unkruer B, Stein V, Bankstahl JP, Soerensen J, Tipold A, *et al.* Over-expression of P-glycoprotein in the canine brain following spontaneous status epilepticus. Epilepsy Res. 2009;83(2–3):144–51.
13. Haslam IS, Jones K, Coleman T, Simmons NL. Rifampin and digoxin induction of MDR1 expression and function in human intestinal (T84) epithelial cells. Br J Pharmacol. 2008;154(1):246–55.
14. Dorner B, Kuntner C, Bankstahl JP, Bankstahl M, Stanek J, Wanek T, *et al.* Synthesis and small-animal positron emission tomography evaluation of [11C]-elacridar as a radiotracer to assess the distribution of P-glycoprotein at the blood-brain barrier. J Med Chem. 2009;52(19):6073–82.
15. Langer O, Bauer M, Hammers A, Karch R, Pataraia E, Koepp MJ, *et al.* Pharmacoresistance in epilepsy: a pilot PET study with the P-glycoprotein substrate R-[(11)C]verapamil. Epilepsia. 2007;48(9):1774–84.
16. Choy G, Choyke P, Libutti SK. Current advances in molecular imaging: noninvasive *in vivo* bioluminescent and fluorescent optical imaging in cancer research. Mol Imaging. 2003;2(4):303–12.
17. Kaijzel EL, van der Pluijm G, Lowik CW. Whole-body optical imaging in animal models to assess cancer development and progression. Clin Cancer Res. 2007;13(12):3490–7.
18. Ntziachristos V, Bremer C, Weissleder R. Fluorescence imaging with near-infrared light: new technological advances that enable *in vivo* molecular imaging. Eur Radiol. 2003;13(1):195–208.
19. Klohs J, Wunder A, Licha K. Near-infrared fluorescent probes for imaging vascular pathophysiology. Basic Res Cardiol. 2008;103 (2):144–51.
20. Hilderbrand SA, Weissleder R. Near-infrared fluorescence: application to *in vivo* molecular imaging. Curr Opin Chem Biol. 2010;14(1):71–9.
21. Miller DW, Fontain M, Kolar C, Lawson T. The expression of multidrug resistance-associated protein (MRP) in pancreatic adenocarcinoma cell lines. Cancer Lett. 1996;107(2):301–6.
22. Martin C, Berridge G, Higgins CF, Callaghan R. The multi-drug resistance reversal agent SR33557 and modulation of vinca alkaloid binding to P-glycoprotein by an allosteric interaction. Br J Pharmacol. 1997;122(4):765–71.
23. Polli JW, Wring SA, Humphreys JE, Huang L, Morgan JB, Webster LO, *et al.* Rational use of *in vitro* P-glycoprotein assays in drug discovery. J Pharmacol Exp Ther. 2001;299(2):620–8.
24. Jonker JW, Wagenaar E, van Deemter L, Gottschlich R, Bender HM, Dasenbrock J, *et al.* Role of blood-brain barrier P-glycoprotein in limiting brain accumulation and sedative side-effects of asimadoline, a peripherally acting analgaesic drug. Br J Pharmacol. 1999;127(1):43–50.
25. Lazarowski A, Czornyj L, Lubienieki F, Girardi E, Vazquez S, D'Giano C. ABC transporters during epilepsy and mechanisms underlying multidrug resistance in refractory epilepsy. Epilepsia. 2007;48 Suppl 5:140–9.
26. Loscher W, Potschka H. Role of multidrug transporters in pharmacoresistance to antiepileptic drugs. J Pharmacol Exp Ther. 2002;301(1):7–14.
27. Zidan AS, Spinks C, Fortunak J, Habib M, Khan MA. Near-infrared investigations of novel anti-HIV tenofovir liposomes. AAPS J. 2010;12(2):202–14.
28. Wang Q, Yang H, Miller DW, Elmquist WF. Effect of the p-glycoprotein inhibitor, cyclosporin A, on the distribution of rhodamine-123 to the brain: an *in vivo* microdialysis study in freely moving rats. Biochem Biophys Res Commun. 1995;211 (3):719–26.
29. Yumoto R, Murakami T, Nakamoto Y, Hasegawa R, Nagai J, Takano M. Transport of rhodamine 123, a P-glycoprotein substrate, across rat intestine and Caco-2 cell monolayers in the presence of cytochrome P-450 3A-related compounds. J Pharmacol Exp Ther. 1999;289(1):149–55.
30. Fontaine M, Elmquist WF, Miller DW. Use of rhodamine 123 to examine the functional activity of P-glycoprotein in primary cultured brain microvessel endothelial cell monolayers. Life Sci. 1996;59(18):1521–31.
31. Horio M, Chin KV, Currier SJ, Goldenberg S, Williams C, Pastan I, *et al.* Transepithelial transport of drugs by the multidrug transporter in cultured Madin-Darby canine kidney cell epithelia. J Biol Chem. 1989;264(25):14880–4.
32. Zhang Y, Bachmeier C, Miller DW. *In vitro* and *in vivo* models for assessing drug efflux transporter activity. Adv Drug Deliv Rev. 2003;55(1):31–51.
33. Shaik N, Giri N, Pan G, Elmquist WF. P-glycoprotein-mediated active efflux of the anti-HIV1 nucleoside abacavir limits cellular accumulation and brain distribution. Drug Metab Dispos. 2007;35(11):2076–85.
34. Giacomini KM, Huang SM, Tweedie DJ, Benet LZ, Brouwer KL, International Transporter Consortium. Membrane transporters in drug development. Nat Rev Drug Discov. 2010;9 (3):215–36.
35. Urbatsch IL, al-Shawi MK, Senior AE. Characterization of the ATPase activity of purified Chinese hamster P-glycoprotein. Biochemistry. 1994;33(23):7069–76.
36. Bachmeier CJ, Trickler WJ, Miller DW. Comparison of drug efflux transport kinetics in various blood-brain barrier models. Drug Metab Dispos. 2006;34(6):998–1003.
37. Syvanen S, Luurtsema G, Molthoff CF, Windhorst AD, Huisman MC, Lammertsma AA, *et al.* (R)-[11C]verapamil PET studies to assess changes in P-glycoprotein expression and functionality in rat blood-brain barrier after exposure to kainate-induced status epilepticus. BMC Med Imaging. 2011;11:1.
38. Tanaka E, Choi HS, Fujii H, Bawendi MG, Frangioni JV. Image-guided oncologic surgery using invisible light: completed pre-clinical development for sentinel lymph node mapping. Ann Surg Oncol. 2006;13(12):1671–81.

39. Urquhart BL, Kim RB. Blood-brain barrier transporters and response to CNS-active drugs. Eur J Clin Pharmacol. 2009;65 (11):1063–70.
40. Rao VV, Dahlheimer JL, Bardgett ME, Snyder AZ, Finch RA, Sartorelli AC, *et al.* Choroid plexus epithelial expression of MDR1 P glycoprotein and multidrug resistance-associated protein contribute to the blood-cerebrospinal-fluid drug-permeability barrier. Proc Natl Acad Sci USA. 1999;96(7):3900–5.
41. de Lange EC. Potential role of ABC transporters as a detoxification system at the blood-CSF barrier. Adv Drug Deliv Rev. 2004;56(12):1793–809.
42. Bigotte L, Olsson Y. Cytotoxic effects of adriamycin on the central nervous system of the mouse–cytofluorescence and electron-microscopic observations after various modes of administration. Acta Neurol Scand Suppl. 1984;100:55–67.
43. Dombrowski SM, Desai SY, Marroni M, Cucullo L, Goodrich K, Bingaman W, *et al.* Overexpression of multiple drug resistance genes in endothelial cells from patients with refractory epilepsy. Epilepsia. 2001;42(12):1501–6.
44. Lin JH. Transporter-mediated drug interactions: clinical implications and *in vitro* assessment. Expert Opin Drug Metab Toxicol. 2007;3(1):81–92.